WL-TR-91-4089

CHARACTERIZATION OF CHOLESTERIC CYCLIC SILOXANE LIQUID CRYSTALLINE MATERIALS

Timothy J. Bunning
Herbert E. Klei
Dept. of Chemical Engineering
University of Connecticut
Storrs, CT 06268

Edward T. Samulski
Dept. of Chemistry
University of North Carolina
Chapel Hill, NC 27599

W.W. Adams
R.L. Crane
Laser Hardened Materials Tech Group
Hardened Materials Branch

November1991

Interim Report for the Period July 1989 - June 1991

Materials Directorate
Wright Laboratory
Air Force Systems Command
Wright-Patterson Air Force Base, Ohio 45433-6533

NOTICE

When Government drawings, specifications, or other data are used for any purpose other than in connection with a definitely Government-related procurement, the United States Government incurs no responsibility or any obligation whatsoever. The fact that the Government may have formulated or in any way supplied the said drawings, specifications, or other data, is not to be regarded by implication, or otherwise in any manner construed, as licensing the holder, or any other person or corporation; or as conveying any rights or permission to manufacture, use, or sell any patented invention that may in any way be related thereto.

This report is releasable to the National Technical Information Service (NTIS). At NTIS, it will be available to the general public, including foreign nations.

This technical report has been reviewed and is approved for publication.

R L Crane

ROBERT L. CRANE, WUD 26 Leader
Hardened Materials Branch
Electromagnetic Mat'ls & Surv Div

Gary K. Waggoner

GARY K. WAGGONER, Chief
Hardened Materials Branch
Electromagnetic Mat'ls & Surv Div

FOR THE COMMANDER

William R Woody

WILLIAM R. WOODY, Chief
Electromagnetic Mat'ls & Surv Div

If your address has changed, if you wish to be removed from out mailing list, or if the addressee is no longer employed by your organization, please notify WL/MLPJ, Wright-Patterson AFB OH 45433-6533 to help us maintain a current mailing list.

Copies of this report should not be returned unless return is required by security considerations, contractual obligations, or notice on a specific document.

REPORT DOCUMENTATION PAGE

Form Approved
OMB No. 0704-0188

1. AGENCY USE ONLY (Leave blank)	2. REPORT DATE	3. REPORT TYPE AND DATES COVERED
	4 Nov 91	Interim July 89- June 91

4. TITLE AND SUBTITLE
Characterization of Cholesteric Cyclic Siloxane Liquid Crystalline Materials.

5. FUNDING NUMBERS
PE: 62102F
PR: 2422
TA: 04
WU: 01

6. AUTHOR(S)
TJ Bunning, HR Klei, ET Samulski, RL Crane, WW Adams

7. PERFORMING ORGANIZATION NAME(S) AND ADDRESS(ES)
Materials Directorate
Wright Laboratory, WL/MLPJ
Wright Patterson AFB OH 45433-6533

8. PERFORMING ORGANIZATION REPORT NUMBER
WL-TR-91-4089

9. SPONSORING/MONITORING AGENCY NAME(S) AND ADDRESS(ES)
Materials Directorate
Wright Laboratory, WL/MLPJ
Wright-Patterson AFB OH 45433-6533

10. SPONSORING/MONITORING AGENCY REPORT NUMBER
WL-TR-91-4089

11. SUPPLEMENTARY NOTES

12a. DISTRIBUTION/AVAILABILITY STATEMENT
Approved for public release; Distribution Unlimited.

12b. DISTRIBUTION CODE

13. ABSTRACT (Maximum 200 words)

The preliminary investigation of a new type of a liquid crystalline material is described. These cyclic cholesteric siloxanes exhibit selective reflection which can be varied from the UV to the NIR by changing composition. DSC, TGA, SEM, TEM, UV-VIS-NIR spectroscopy, & polarized optical microscopy (POM) were used to obtain preliminary information on the thermal, optical and macroscopic packing behavior as it related to possible optical applications of these materials. Considerable effort was also employed in examining the wide-angle & small-angle X-ray scattering (WAXS & SAXS) patterns obtained from these materials in a variety of forms including film, fiber, & powder samples.

14. SUBJECT TERMS
Liquid Crystal — X-Ray Diffraction
Cholesteric — Electron Microscopy
Siloxane Smectic — Spectroscopy

15. NUMBER OF PAGES
73

16. PRICE CODE

17. SECURITY CLASSIFICATION OF REPORT	18. SECURITY CLASSIFICATION OF THIS PAGE	19. SECURITY CLASSIFICATION OF ABSTRACT	20. LIMITATION OF ABSTRACT
UNCLASSIFIED	UNCLASSIFIED	UNCLASSIFIED	UNLIMITED

FOREWORD

The following report was prepared under the AFOSR Laboratory Graduate Fellowship Program (LGFP) under Contract F49620-86-C-0127. The work was initiated under Project No. 2422, "Laser Hardened Materials", Task No. 0401, Work Unit Directive (WUD) 26. It was administered under the direction of the Materials Directorate, Wright Laboratory, Air Force Systems Command, Wright-Patterson Air Force Base, Ohio with Dr. R.L. Crane as the Materials Directorate Project Scientist (WUD Leader). Coauthors were Timothy J. Bunning, Dept. of Chemical Engineering, University of Connecticut, on leave as a Ph.D. Doctoral Candidate under the LGFP program, Dr. H.E. Klei, Dept. of Chemical Engineering, University of Connecticut and Dr. E.T. Samulski, Dept. of Chemistry, University of North Carolina, whom serve as academic advisers to TJB, and Dr. R.L. Crane and Dr. W.W. Adams, Materials Directorate (WL/MLPJ). This report covers research conducted from 1 July 1989 to 30 June 1991.

The authors thank Mr. Gary Price, University of Dayton Research Institute, for technical assistance and Dr. Allen Wachtel, Biology Dept., University of Connecticut for assistance with the SEM and TEM research.

TABLE OF CONTENTS

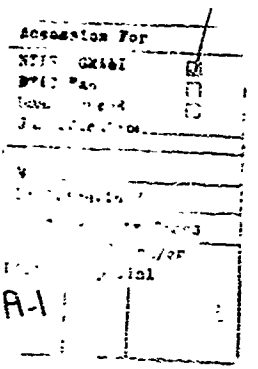

LIST OF TABLES

Section 1
INTRODUCTION

Currently, the Materials Directorate Laser Hardened Materials Branch is conducting an in-house research program centered on aligned organic structures for nonlinear optical applications. Organic materials exhibiting high nonlinear optical (NLO) behavior [1,2] have shown promise in a variety of optical devices. Optically NLO materials are currently being examined due to their applicability in controlling and manipulating the temporal, spatial, and frequency properties of light [3]. Because ordering of the NLO chromophore can give rise to large response amplitudes, one system currently being investigated are liquid crystalline materials which inherently possess order on a molecular scale.

Liquid crystalline materials may be defined as a thermodynamically stable bulk state of matter with a degree of internal order intermediate that of isotropic fluids and crystalline solids. This yields materials which combine the viscosity, elastic properties, dielectric properties, and response times of a liquid with the long-term order and birefringence characteristic of crystalline materials. Thus these materials exhibit anisotropy in their mechanical, electrical, magnetic, and optical properties.

The three-dimensional order present within a crystalline solid usually breaks down when heated to its melting point to yield an isotropic liquid where the molecules tumble and rotate freely. Thermotropic materials instead undergo an incremental melting where upon heating there is a systematic breakdown in the

molecular order as shown in Figure 1. This controlled melting is driven by the anisotropy and chemical structure of the molecules. These phases are thermodynamically stable and thus have to be considered as a separate phase of matter intermediate between a liquid and a solid. Thermotropic mesophases may occur over a broad range of temperatures permitting the fabrication of temperature dependent materials.

The breakdown in order with temperature has historically been used to classify thermotropic liquid crystals. Rod- or lath-shaped molecules can be divided into two main classifications: nematic and smectic. Nematic liquid crystals have lost all positional order and only maintain orientational order due to the molecule's physical anisotropy (Figure 2(a)). The average direction of the molecular long axes can be represented by a unit vector. The centres of mass of these molecules are free to translate in any direction thus forming an anisotropic liquid. The incorporation of a chiral center into a nematic-forming molecule will result in the formation of a cholesteric mesophase. Although this mesophase only has orientational order, the unit director is rotated in space yielding a material which has an optic axis perpendicular to the plane of the molecules (Figure 2(b)). The mesophase can thus be modeled as sheets of nematic liquid crystals where each layer is slightly rotated with respect to each other. The distance it takes for the director to rotate 360° is defined as the pitch.

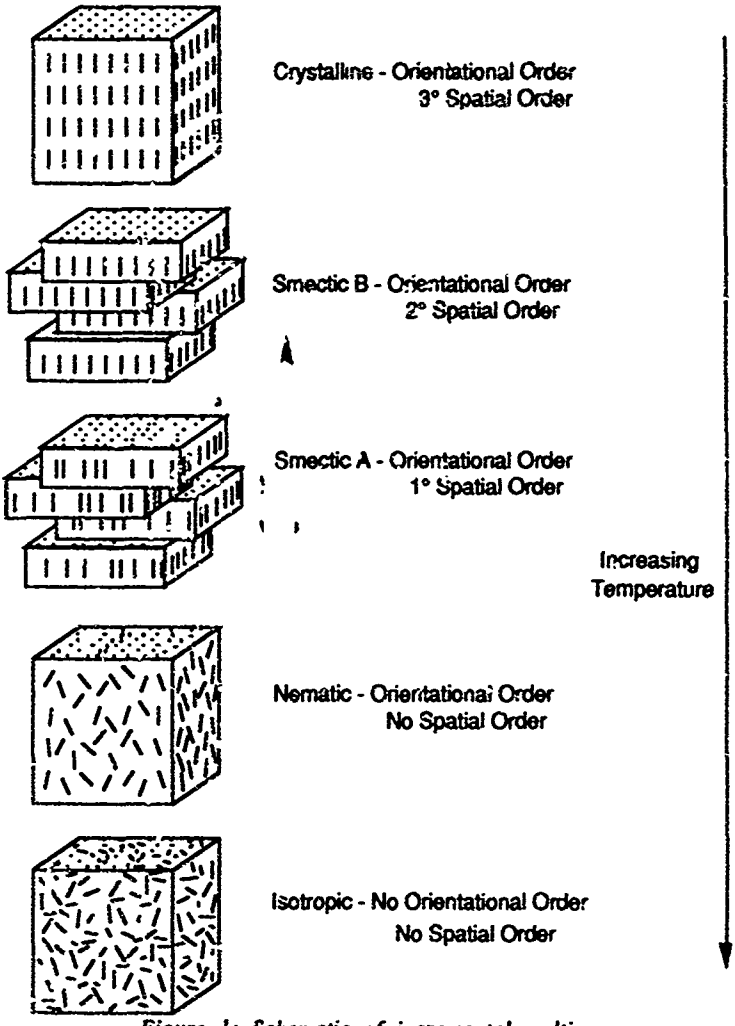

Figure 1: Schematic of incremental melting process of anisotropic molecules

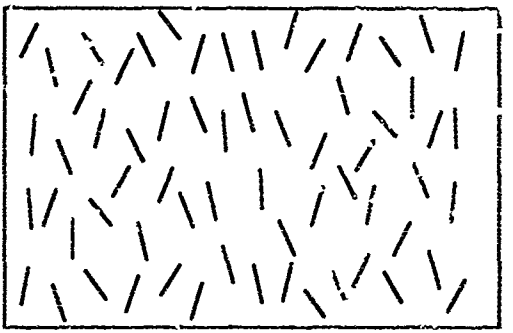

(a)

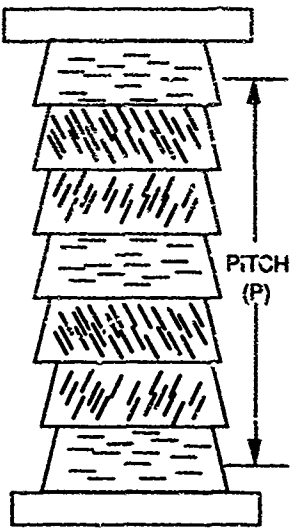

(b)

Figure 2: Nematic (a) and cholesteric (b) liquid crystal orientation

The second major classification for lathe-shaped molecules are the smectic mesophases. This class of materials has at least one degree of positional order as well as the orientational order present with nematics. Although there are at least nine different smectic classifications, the most common mesophases are shown in Figure 3. Smectic A materials pack in a layered form although the layers freely slide over one another and the molecules are free to rotate and traverse within the layers. Smectic B layers are similar except they have hexagonal order within the layers. Again, the molecules are free to rotate, and the layers are free to slide over one another. The smectic C mesophase is the tilted analog of the smectic A mesophase, and these can exhibit unique optical properties when the molecules are chiral.

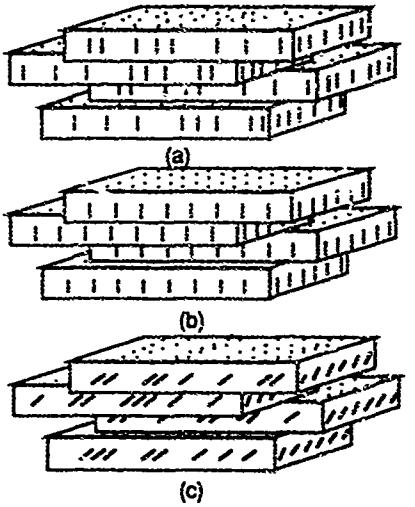

Figure 3: Common smectic mesophases: (a) smectic A, (b) smectic B, and (c) smectic C

One liquid crystalline system currently being examined is the cyclic siloxane-based materials which are ordered on both the microscopic and macroscopic scale. The preliminary materials examined were pentamethylcyclopentasiloxane rings with pendant mesogenic groups attached as shown in Figure 4. These materials consist of a cyclic siloxane core with two different mesogenic groups attached through appropriate groups. These mesogens, cholesterol and biphenyl, were connected to the siloxane rings by allyloxybenzoic acid leader groups. These materials (Wacker L.C. Silicones) were produced by Wacker Chemie and supplied by Dr. F. H. Kreuzer of the Consortuim fur Elektrochemische Industrie GmbH. Although shown in Figure 4 as consisting of one ring size, it has been shown by Krishnamurthy [4] that these materials consist of a variety of ring sizes with 5 being the predominant size.

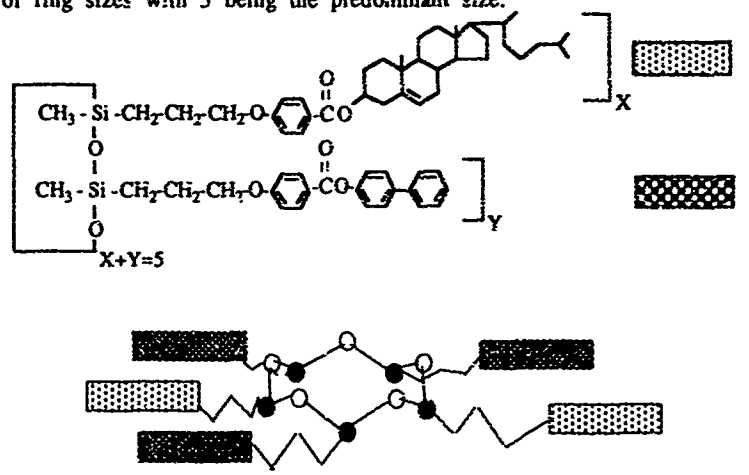

Figure 4: Schematic of cyclic siloxane ring with mesogenic groups attached through appropriate leaders

Due to the chiral nature of the cholesterol molecule, these materials form a cholesteric liquid crystal and thus selectively reflect circularly polarized light at a given wavelength. By changing the ratio of the cholesterol to biphenyl content, this reflection wavelength can be varied from the ultraviolet (UV) to the near infrared (NIR). Table 1 lists the four compounds examined with their selective reflection wavelengths and the statistical mole fraction of cholesterol mesogen within the ring based on a 5-membered ring.

Table 1

Wacker LC-Siliconea Investigated

Compound #	X_{chol}	λ_{max} (nm)
1	0.40	440
2	0.36	515
3	0.31	610
4	0.14	1190

Several groups have exploited the optical properties of these materials including Tsai et al. [5] who developed a laser notch filter centered in the visible spectra, Pinsl et al. [6] who developed a write-once-read-many (WORM) optical storage material, and Ortler et al. [7] who has developed a reversible read-write organic holographic optical data storage material. These applications take advantage of the liquid crystalline order on a macroscopic scale. Preliminary X-ray investigations [8] have also indicated a high degree of order on a molecular scale uncharacteristic of liquid crystalline materials. This report details the characterization of the four materials listed in

Table 1 using Differential Scanning Calorimetry (DSC), Thermal Gravimetric Analysis (TGA), Scanning and Transmission Microscopy (SEM/TEM), ultraviolet-visible-near infrared spectroscopy (UV-VIS-NIR), and polarized optical microscopy (POM). These four characterization methods were used to obtain preliminary information on the thermal, optical, and macroscopic packing behavior as it relates to possible applications of these materials as organic optical materials. X-ray diffraction techniques were also employed to examine the molecular packing behavior of these materials. Emphasis was placed on interpreting unique Wide-Angle and Small-Angle X-ray Scattering (WAXS and SAXS) patterns obtained from these materials in a variety of forms including film, fiber, and powder samples.

Section II

METHODS

X-ray Diffraction

X-ray diffraction experiments were performed on either a Rigaku RU-300 (operated at 12kW at 40kV, 300mA) or a Rigaku RU-200 (operated at 12kW at 60 kV, 200mA) rotating anode generator using CuKα radiation (graphite monochromator). Transmission photographs were recorded with an evacuated Statton Camera (flat film) using various sample-to-film distances including 50 mm, 72.9 mm and 170 mm. Several samples were also examined with a Philips X-ray microcamera equipped with a 2-mil collimator. D-spacing calibrations were performed with the National Bureau of Standard's Reference Material 640 (Si powder). Elevated temperature work was performed on capillaries packed with the powered material in a homemade heating block fitted to the inside of the Statton camera. The heater was powered with a variable voltage source and temperature was monitored with an Omega 650 Type J thermocouple.

Films of the materials were obtained by shearing the material between two Teflon sheets. These sheets were sandwiched between two microscope slides and subsequent movement of one over the other caused sudden orientation of the material into its Grandjean (planar) packing state. Film shearing was performed in the liquid crystalline phase at elevated temperatures of 130-150°C on a hot plate. Upon removal of the film from the heat source, ambient air

coooling quenched the material into a glass. Although glassy, the liquid crystalline order was frozen into the thin films.

An interesting property of these materials was their ability to be drawn into fibers, although they do not contain long extended polymeric backbones. Typically associated with polymeric materials, fiber drawing occurs because of to the high degree of longitudinal interactions caused by covalent bonding of nearest neighbors over many atoms which hold the material together. This allows polymeric materials to be stretched, thereby forming an array of extended polymer chains. Low molecular weight materials typically are held together only by weak intermolecular forces such as Van der Waals interactions and therefore cannot withstand the tensile forces when drawn.

Fibers were drawn from these materials by pulling strands of various diameters with a spatula from the liquid crystalline melt (130-150°C). These fibers quickly cooled in air. Although brittle at room temperature owing to their glassy texture, fibers of long length (tens of meters) could be drawn from the liquid crystal mesophase rather easily.

Thermal Analysis

Differential Scanning Calorimetry (DSC) was performed on either a Perkin-Elmer DSC-2C equipped with a Thermal Analysis Data Station or a Dupont 910 DSC equipped with an OMNITHERM ATVANTAGE II controller. All reported transition values were taken from the second of two heating scans so that each sample had the same thermal history.

Thermal Gravimetric Analysis (TGA) was performed on a Dupont TGA controlled with an OMNITHERM 35053 controller. Samples were run in air. Mass spectroscopy was performed on the degradation products by Systems Research Laboratories through MLBP (Polymer Branch).

Polarized Optical Microscopy

Polarized optical microscopy (POM) was performed on a Nikon Optiphot-Pol microscope equipped with a Microflex UFX-II photomicrographic attachment. Photographs were taken with either a Nikon FX-35WA 35 mm camera or a Polaroid Model 545 4x5 film holder. Other color prints were obtained with a Javelin color video thermal printer. A Panasonic WV-6000 color video camera attached to the microscope was used to obtain images for the thermal printer.

Hot stage microscopy was performed with a Fryer A-200 temperature controller. Powdered material was placed between two cover glass slips and heated to the desired temperature. Glassy film and fiber samples were also examined at room temperature on glass substrates.

UV-VIS-NIR Spectroscopy

The visible optical properties (selective reflection and scattering) were examined with a Perkin-Elmer Lambda 4B UV/VIS spectrophotometer and a Lambda 9 UV-VIS spectrophotometer. The Lambda 4B was equipped with an integrating sphere which allowed the specular reflection to be measured. The optical properties in the

near infrared region were examined with a Perkin-Elmer Lambda 9 UV/VIS/NIR spectrophotometer.

Samples to be examined were sheared between microscope slides on a hot plate at 150°C. The microscope slides were cleaned with toluene before use. The material was sheared to align the cholesteric helices and then cooled in air. Spectra were taken with the light propagation direction normal to the glass slides. A blank substrate spectrum was subtracted from the sample spectrum. Films (foils) of the Wacker LC-Silicones sheared on black paper obtained from F.H. Kreuzer [9] were examined in the reflection mode. Sheared samples between glass slides were measured in the absorption mode. Since these materials do not absorb in the visible, the absorption spectra were almost identical to the reflection spectra. All slides examined were annealed for 72 hours at 120-130°C after the initial scan to obtain the same thermal history. Values for λ_o and $\Delta\lambda_{(FWHM)}$ were compared before and after annealing.

Scanning and Transmission Electron Microscopy (SEM/TEM)

SEM was performed on either an HP550B Coates and Welter field emission SEM equipped with a cold cathode (at the University of Connecticut) or a Hitachi S-900 SEM equipped with a field emission gun and an immersion lens system (at MLLM characterization facility). This latter instrument allowed for very low operating voltages to be employed enabling microstructures to be recorded without having to coat a conductive layer of metal on the surface to be examined. A freeze-fracture technique was employed with both film and fiber samples. This consisted of immersing the sample in

liquid nitrogen followed by fracturing along the desired axis. Annealed fiber samples were prepared by floating them on water at 70-80°C until the desired shrinkage was obtained. These fibers were then cooled in ice water and fractured.

TEM was performed with a Philips 300 electron micrscope. Samples investigated were embedded within an epoxy matrix and thin samples (<1000 Å) were microtomed with a diamond knife. The original epoxy system needed an elevated temperature (60-70°C) to cure. This heating was observed to shrink the sample thereby destroying the alignment of the cholesteric helices. A second room temperature curing epoxy system was subsequently employed in the preparation of the TEM samples.

Section III

THERMAL CHARACTERIZATION

The glass transition (T_g) and clearing temperatures (T_{cl}) for the four Wacker LC-Silicone products examined are listed in Table 2. These values fall within the reported [10] ranges of 40-50°C for the T_g and 180-210°C for the T_{cl} obtained with the materials. A typical DSC scan is shown in Figure 5.

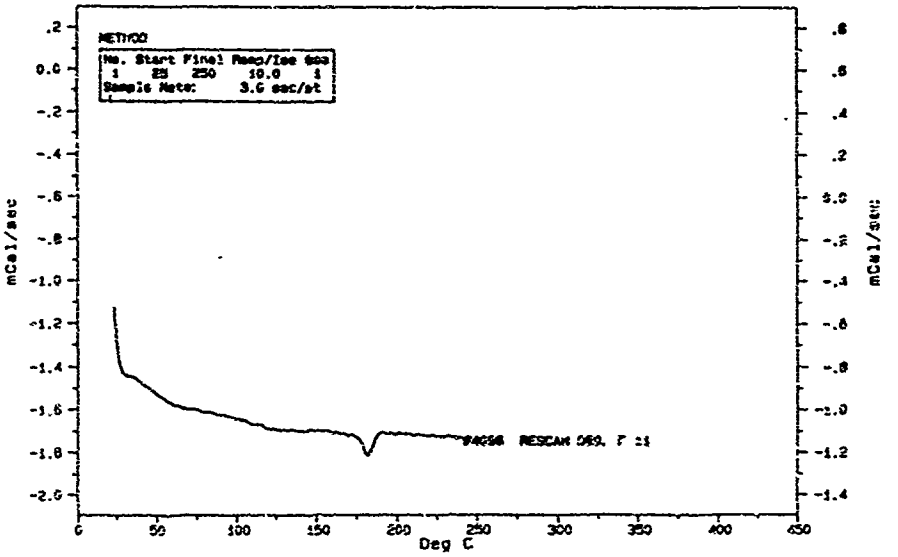

Figure 5: Typical DSC scan for these l.c. materials

Table 2

Thermal Transitions of Wacker LC-Silicones

Compound	T_g (°C)	T_{cl} (°C)
1	44.0	196.2
2	45.1	206.3
3	42.4	191.3
4	47.3	182.9

TGA revealed a three-step degradation process in air. Mass spectroscopy of the degradation products revealed fragments were released primarily at two temperatures, 335°C and 440°C. Comparisons between compounds 1 and 4 reveal that 11% of the initial sample weight for compound 4 and 55% of the initial sample weight for compound 1 is lost at 335°C. This difference is due to the increased mole fraction of cholesterol in compound 1. Thus, the breakup of the cholesterol-containing pendant group accounts for the low temperature fragments. Also noted was the poor agreement between weight loss and volatile-product detection in compound 1 which was an indication of sublimation. This indicates the cholesterol mesogens were less stable than the biphenyl mesogens when heated in air.

Section IV

UV-VIS-NIR SPECTROSCOPY RESULTS

The selective reflection wavelengths shown in Table 1 were measured using UV-VIS-NIR spectroscopy on sandwiched films using glass as the substrates. The behavior of unpolarized radiation incident normal to an aligned cholesteric film is represented in Figure 6. If the pitch of the material is such that the wavelength obtained from equation 1 is the same wavelength as the unpolarized radiation, half the radiation will be reflected with the other half being transmitted. The handedness of the reflected radiation is the same as that of the material. Opposite handedness radiation is transmitted unaffected. The reflection bandwidth is governed by equation 2.

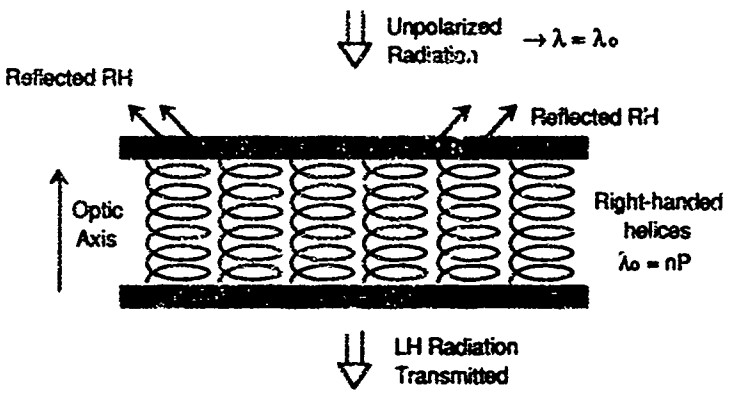

Figure 6: Schematic of selective reflection behavior from aligned cholesteric helices

$$\lambda = n * P \qquad \text{Eq. 1}$$

$$\Delta\lambda = \Delta n * P \qquad \text{Eq. 2}$$

In these equations, n is the average index of refraction, P is the pitch of the helix (distance (see Figure 2) it takes the director to traverse 360°), Δn is the birefringence, λ is the selective reflection wavelength, and $\Delta\lambda$ is the bandwidth of the reflection band. These equations have been developed based on the pioneering work of DeVries [11]. When the pitch of the helices are on the order of the wavelength of visible light, these materials become highly iridescent.

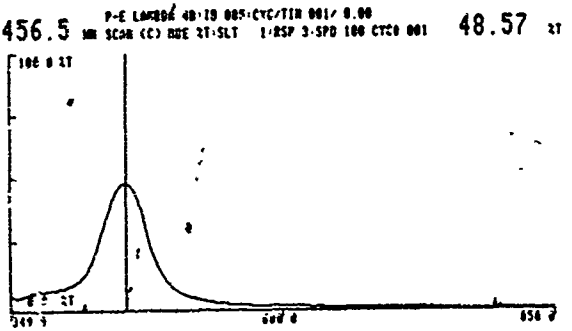

Figure 7: Typical reflection spectra of compound 1

Figure 7 shows a typical reflection spectra obtained with an integrating sphere attached to a UV-VIS spectrophotometer. It should be noted that these materials have little absorption outside

the reflection band through the entire visible region and therefore normal transmission or absorption spectroscopy can be used to obtain the results shown in Figure 7.

Interestingly, the reflection wavelength and bandwidth were observed to be partially controllable by thermal annealing in an oven near the clearing points of the materials sandwiched between glass substrates. Table 3 shows both the reflection wavelength and bandwidth for the visibly reflecting materials both before and after annealing. Annealing was performed at 120-130°C for 72 hours.

Table 3

Annealing Results on Wavelength and Bandwidth

	Before Annealing		After Annealing		Change	
Sample	λ (nm)	Δλ (nm)	λ (nm)	Δλ (nm)	λ (nm)	Δλ (nm)
1	475	77	440	68	-35	-9
2	553	112	515	93	-38	-19
3	674	133	610	117	-64	-16

As Table 3 shows, the reflection wavelength was shortened and the reflection bandwidth shrank with annealing. This behavior was attributed to an increase in the packing behavior of the liquid crystalline mesogens allowing a better continuity from layer to layer which subsequently shortens the pitch. Examinations were also

conducted at an annealing temperature of 90°C but very small changes in the reflection wavelength were observed. However, comparable changes in the reflection bandwidth were observed. Investigations with the top substrate removed resulted in similar changes to the reflection behavior. The resulting wavelengths and bandwidths were stable at room temperature indefinitely. These results indicate the possibility of "tuning" both the reflection wavelength and bandwidth by controlled annealing for given period of time.

Also measured were the reflection wavelengths obtained from these three materials coated on black paper as supplied by Dr. F.H. Kreuzer. Cross-sections of these films were also investigated with SEM which allowed for direct visual measurement of the pitch distances. Armed with these two figures, the average index of refraction as given in Eq. 1 can be calculated. These results will be discussed in Section VI.

Section V

OPTICAL MICROSCOPY RESULTS

Optical microscopy was used to examine the phase behavior of these materials as well as the homogeneity of the isotropic liquids. Crossed polarizing microscopy clearly indicated one of two types of textures at elevated temperatures characteristic of cholesteric materials. Figure 8 shows a typical focal-conic texture characteristic of random orientation of the helical axes through the film. Upon movement of the top cover glass slip, sudden orientation of the helices occurs which aligns the material into its Grandjean (planar) state. This texture is responsible for the selective reflection behavior as observed in Figures 6 and 7. Under crossed polarizers, this aligned packing orientation exhibits a characteristic "oily" texture as shown in Figure 9.

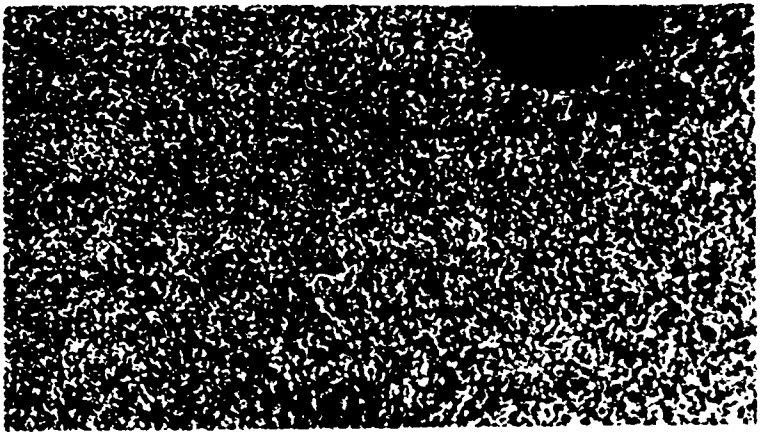

Figure 8: Characteristic focal-conic texture as observed with optical microscopy (200 X)

Figure 9: Characteristic planar texture as seen with optical microscopy (200 X)

The homogeneity of these materials was also examined qualitatively by examining the texture of the liquid crystalline and isotropic phases. These examinations clearly showed the presence of foreign particles within the bulk of the material. This behavior was expected as preliminary TLC examinations showed a number of spots for all materials which indicates impurities. These foreign particles can act as scattering and nucleation sites which disrupt the relative orientation of the helices and thus the optical performance of these materials.

Microscopy was also used to examine the relative birefringence of fibers drawn from these materials. This behavior is unique because of the low molecular weights of these materials. Under crossed polarizers, fibers of all four materials were birefringent. As

Figure 10 shows, when the stage is rotated through 45°, the fibers that were originally dark become light and vice versa. Fibers of compound 1 were much more birefringent than fibers of compound 4.

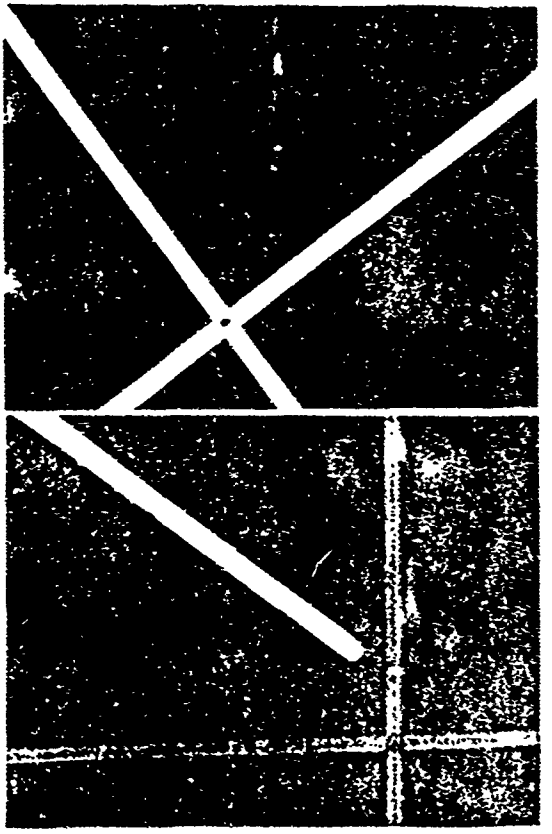

Figure 10: Fibers observed with optical microscopy. Bottom fibers have been rotated 45° with respect to the top fiber (crossed polarizers) (compound 1-fiber diameters~100μm)

Section VI

SEM/TEM RESULTS

The uniformity of the macroscopic packing needed for high optical quality components was examined with both scanning electron microscopy (SEM) and transmission electron microscopy (TEM). Various types of defects present in cholesteric materials, contaminants introduced in the synthesis and handling, and misalignment owing to poor shear conditions can be observed with electron microscopy. Fracture surfaces of an edge geometry from cholesteric materials also reveal a regular lamellar stratification corresponding to the half-helical pitch P/2. This topography is due to the continually changing orientations of the mesogens with respect to the fracture plane as they rotate through the thickness of the film.

Examinations of sheared films from these materials indicate a very good macroscopic alignment of the cholesteric axis with respect to the glass substrates. Fracture surfaces tangent to the cholesteric axis (i.e., edge surfaces formed by fracturing a thin sample) vividly show the Grandjean texture. Figure 11, which shows the entire fracture surface of a film, indicates the spacing of the cholesteric planes was fairly uniform and parallel to the film surface. Higher magnification examinations reveal areas where the alignment was very good and allow for direct measurement of the cholesteric pitch distances (Figure 12). In both of these figures, the lamellar spacing corresponds to a distance of P/2. Even with this apparent uniformity, there is considerable room for improvement as evidenced by the surface layers of Figure 11. The alignment of the

surface layers was not as uniform as in the middle of the fracture surface. This misalignment and the large number of disclinations (liquid crystalline defects) present in the bulk greatly reduce the optical quality and the laser damage thresholds for these materials. The granularity present in Figure 12 was attributed to a conductive coating applied on nonconductive samples with standard SEM techniques. Examinations with the Hitachi low voltage SEM confirmed this behavior as samples viewed with this microscope showed a marked absence of the granularity. Uncoated samples could be examined with this scope because of its low operating voltage.

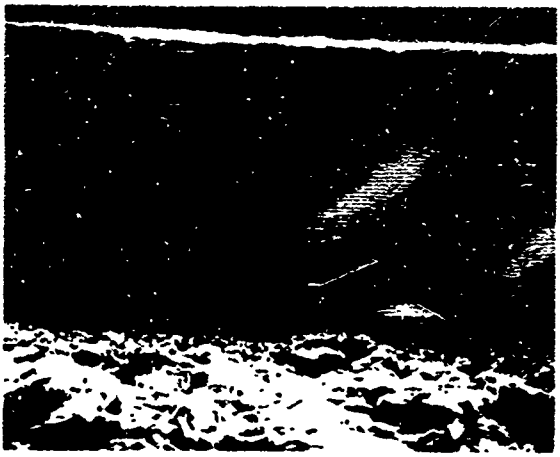

Figure 11: SEM micrograph of cross-section of fractured area (25.4 mm=5 μm)

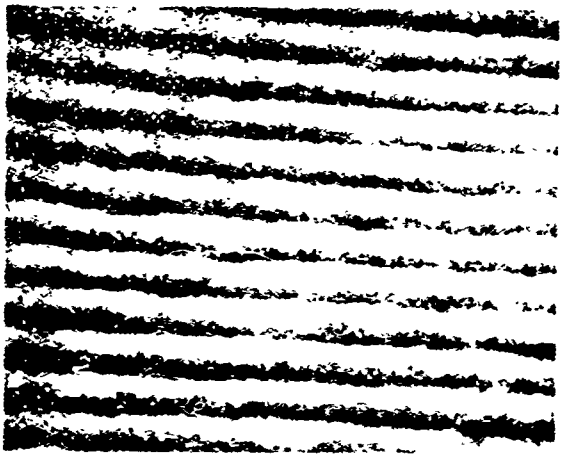

Figure 12: Magnified view of selected area in Figure 11

(6 mm=100 nm)

The actual pitch distances were measured using SEM on compounds 1-3. Great care was taken to ensure that photographs were taken with a viewing angle of 90°. Other work has shown that the resulting fracture pattern observed with electron microscopy is greatly dependent on the viewing angle. Data were obtained by measuring the distance over a number of repeats and then averaging them to obtain an average distance of the pitch. Table 4 shows the measured values of the pitch along with the measured reflective wavelengths obtained for the same samples. This allows the index of refraction of these materials to be calculated. The λ_{max} values were obtained from the thin films on black paper obtained from Dr. F.H. Kreuzer as mentioned in Section IV.

Table 4

Measured Pitch Lengths and Reflection Wavelengths with the Corresponding Calculated Average Index of Refraction

Compound	Pitch (nm)	λ_{max} (nm)	n
1	288	457	1.6
2	335	531	1.6
3	400	652	1.6

Materials that were annealed above their clearing temperatures and then cooled to room temperature without applying shear were also investigated. As Figure 13 shows, the random focal-conic packing of the cholesteric helices was clearly evident. The lines or layers in this figure have an average spacing of P/2 and reveal the periodic layered structure expected of a helical material. This microstructure also shows the randomness of a focal-conic structure. This misalignment of the cholesteric axes results in random reflection (scatter) of light in all directions which results in an optically opaque material.

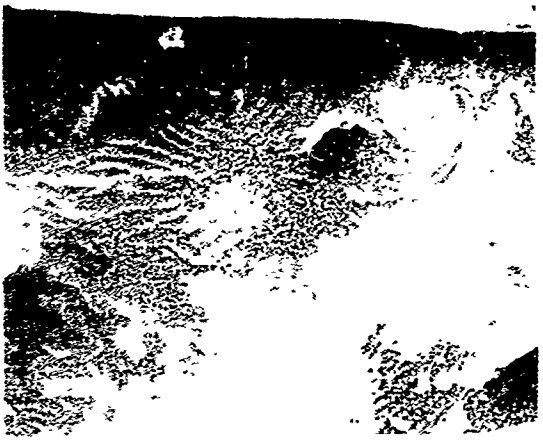

Figure 13: Typical random-conic orientation of helices as observed with SEM (10 mm=1 μm)

The presence of absorbing or scattering particulates within films of these materials ultimately decreases optical quality and lowers laser damage threshold. Figure 14 shows an inclusion of dust within a fracture cross-section of one of these films. This clearly demonstrates the misaligned layers surrounding this inclusion. To produce the clarity that would warrant the use of these materials for optical purposes, the control of orientation in these films must be achieved. This includes the optimization of shear stress during formation of thin films, elimination of inclusions, and achievement of uniform thicknesses in thin films. Using thinner coatings would decrease scattering caused by inclusions because of the lower probability of their occurrence, but this would be partially offset by an increasing amount of surface randomness arising from an

increased volume percentage of this material. Additionally, below a certain thickness the material will not significantly attenuate incoming radiation [12].

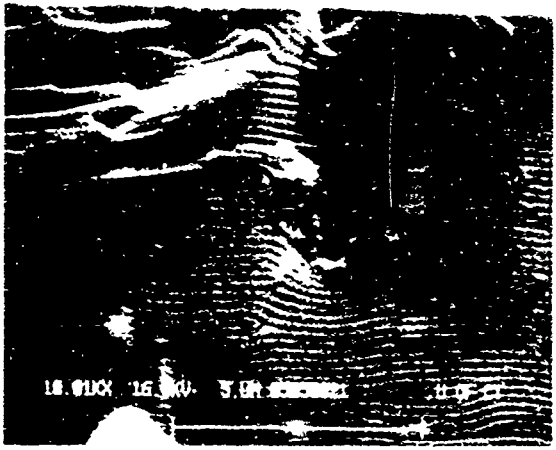

Figure 14: Inclusion present within film as observed with SEM (51 mm=5 μm)

Fibers of various diameters were also examined with electron microscopy (Figure 15). The holes in the surface plane are due to air bubbles being stretched when the fibers are drawn. No evidence of a mature cholesteric texture was observed for thin fractured fibers drawn and quenched from the melt. Figure 16 shows a morphology that does not contain the characteristic lamellar fracture surfaces observed in thin film fracture surfaces. Fibers which were annealed, however, do show the characteristic focal-conic texture although these fibers shrank into a blob during the annealing process. It is

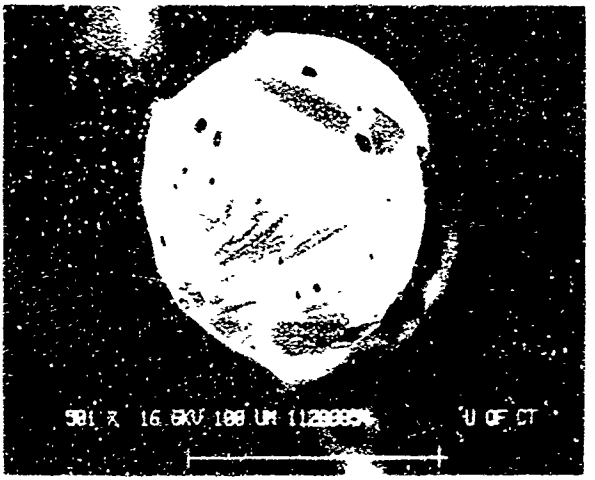

Figure 15: Cross-section of a typical fiber (51 mm=100 μm)

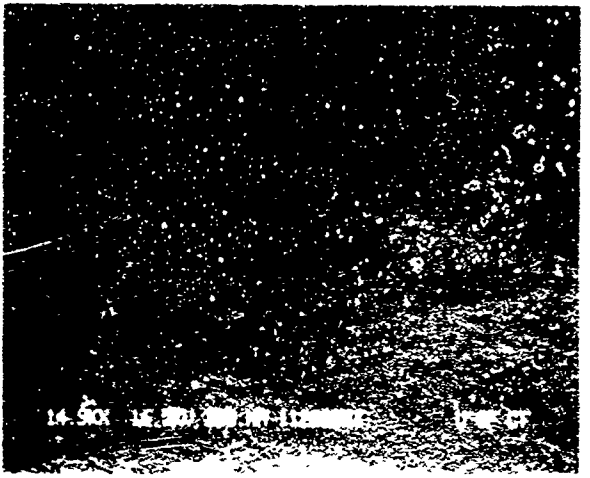

Figure 16: Fiber (unannealed) cross-section fracture exhibiting a featureless morphology

hypothesized for very thin fibers that the high draw stress untwists the helical axis along the length of the fiber and therefore no cholesteric texture is observed. Upon annealing, however, the material relaxes back to its most thermodynamically stable state, the focal-conic packing structure, and this random structure was observed to reappear.

TEM results generally confirm the results of the SEM analysis. Because of the different orientations of the molecules as at twists in its cholesteric state, a series of bright and dark lines were observed with TEM. A typical micrograph, shown in Figure 17, reveals the high degree of contrast among striations. These lines were attributed to the periodic structure of the cholesteric axes and minimum distances between parallel light or dark lines correspond well to the measured spacings obtained with SEM. Since the least transmission of an electron beam makes a dark region on the TEM micrograph, the dark striations correspond to molecules normal to the beam direction, and the white striations correspond to molecules parallel [13]. In analogy to the SEM results, Figure 17 shows regions where a relatively high degree of parallelism among striations indicates good macroscopic order.

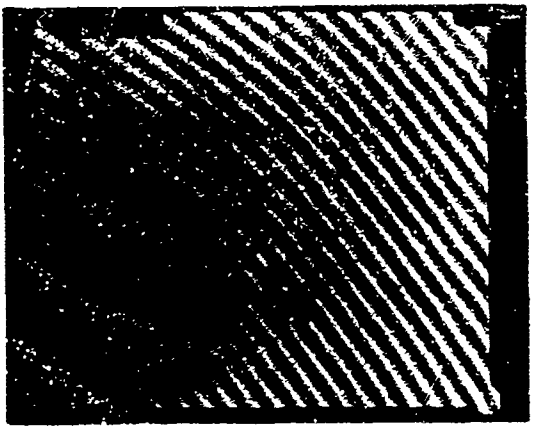

Figure 17: TEM micrograph showing good macroscopic order (25.4 mm=1.2 μm)

Owing to the high degree of contrast, this method is very powerful in examining not only the relative packing structure but also defects including disclinations and dislocations as well as foreign particulate matter embedded within the material. Figure 18 shows a region containing a number of liquid crystalline defect structures.

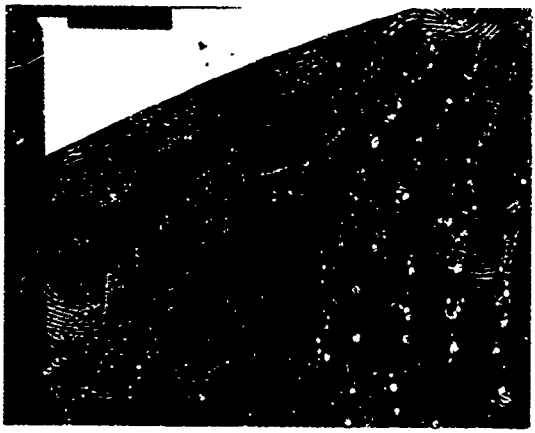

Figure 18: Characteristic TEM photograph showing high contrast resulting from the cholesteric phase behavior (25.4 mm=6.1 μm)

Section VII

X-RAY DIFFRACTION RESULTS

Edge Geometries

Film samples were run in two separate orientations, designated edge and normal as shown in Figure 19. Figures 20-23 show the edge WAXS patterns for all four materials listed in Table 1. The most striking attribute of these diffraction patterns was the higher order layer reflections observed along the meridian. The appearance of these high order reflection lines signifies the presence of a layered structure containing significant order. This behavior is unexpected because these materials were cholesteric (i.e., twisted nematic) and therefore should have no positional order among mesogens.

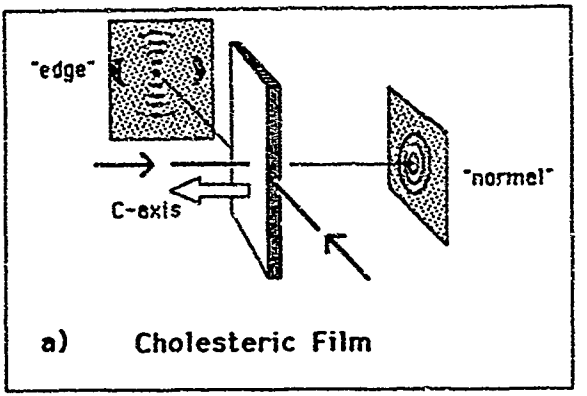

Figure 19: Schematic of X-ray orientations with respect to film edge and normal classifications

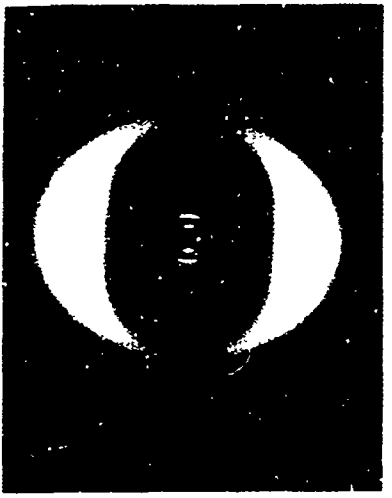

Figure 20: X-ray WAXS pattern from compound 1

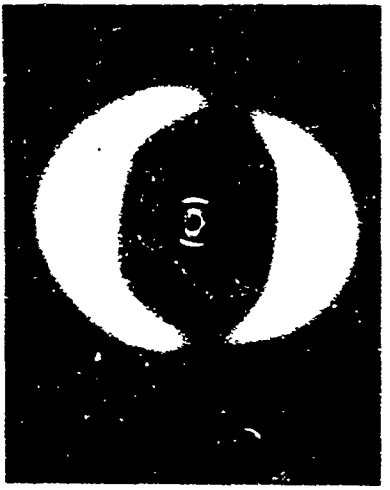

Figure 21: X-ray WAXS pattern from compound 2

Figure 22: X-ray WAXS pattern from compound 3

Figure 23: X-ray WAXS pattern from compound 4

Table 5 shows the observed X-ray reflections from film edges for all four samples. The low angle reflections will be discussed later. Three of these compounds showed four meridional layer lines while compound 4 (x_{chol}=0.14) showed six layer lines. The calculated spacings presented in this table were based on the average value of the primary d-spacings determined from each layer line. As shown, these calculated higher order d-spacings were in good agreement with the observed d-spacings which suggests these spacings were multiple order reflections from a primary layer line. The dependence of the nth order layer lines on x_{chol} also indicates these reflections were multiple order reflections from a primary layer line. These higher order reflections were attributed to a well defined layered smectic-A like structure with long-range positional order of the mesogens [14,15]. Typical smectic-A structures may be modeled using a weak sinusoidal electron density distribution (Figure 24(a)) which usually results in the appearance of only the first order layer line in a diffraction pattern (Figure 24(b)). As shown, long-range order is typically needed for the appearance of higher order d-spacings. The appearance of 5th and 6th order layer lines as in compound 4 suggests these materials were unusually ordered. This order can be represented by layers perpendicular to the film surfaces where mesogens lie within these layers and subsequently in a plane parallel to the surface of a film. This is contrary to a typical twisted nematic model where the mesogens can be represented as lying within a plane parallel to the surface but with no positional order within that plane. The appearance of these

Table 5

X-ray Edge Diffraction Data

x_c=0.40 film (edge)

Meridional spacings, Å	Diffraction order	Calculated spacings **
49.0 (small angle)		
25.4	1	25.0
12.2 (weak)	2	12.5
8.2	3	8.3
6.4 (weak)	4	6.3
Equatorial crescent - 5.1 Å		

x_c=0.36 film (edge)

Meridional spacings, Å	Diffraction order	Calculated spacings **
50.0 (small angle)		
25.0	1	24.6
12.1 (weak)	2	12.3
8.1	3	8.2
6.2 (weak)	4	6.2
Equatorial crescent - 5.0 Å		

Table 5 (con't)

x_c=0.31 film (edge)

Meridional spacings, Å	Diffraction order	Calculated spacings **
50.0 (small angle)		
24.0	1	24.1
12.0 (weak)	2	12.1
8.0	3	8.0
6.1 (weak)	4	6.0
Equatorial crescent - 4.8 Å		

x_c=0.14 film (edge)

Meridional spacings, Å	Diffraction order	Calculated spacings **
-- (no small angle maximum)		
22.3	1	23.2
11.6	2	11.6
7.8	3	7.7
5.8	4	5.8
4.7	5	4.6
3.9	6	3.9
Equatorial crescent - 4.5 Å		

** -- Calculated from average d-spacing obtained from observed layer spacings

multiple order layer lines from film edges, however, indicates long-term positional order of the mesogens within the planes.

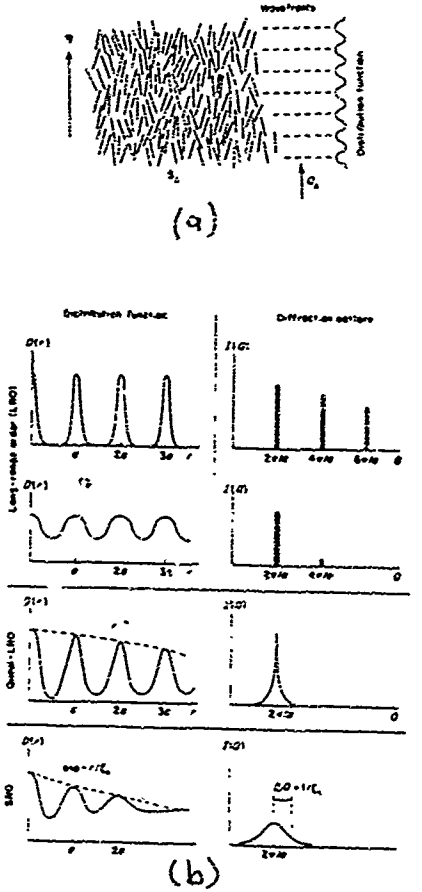

Figure 24: Electron density distribution for typical smectic-A materials and the corresponding X-ray diffraction patterns [16]

Also present in these edge patterns were diffuse equatorial crescents with broad azimuthal distributions which correspond to the lateral intermolecular distances within a single layer. The broad distribution of reflections indicates the liquid-like motion of the mesogens and suggests that these materials have random lateral interactions. This is typical of smectic-A materials (Figure 25) which do not have order within a layer.

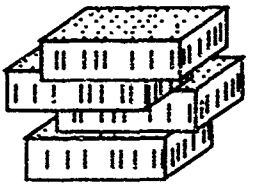

Figure 25: Typical smectic-A liquid crystalline geometry

There was a strong linear correlation of the length of both the primary d-spacings and the lateral distances with respect to mole fraction cholesterol as shown in Figure 26. As the mole fraction of cholesterol increased within the ring system, both the primary d-spacing and lateral distance increased. The latter of these can be attributed to the larger diameter (of a cylinder cut out in space caused by rotation around the primary axis of each mesogen) of the cholesterol mesogen verses the biphenyl mesogen. The linear dependence of the primary d-spacing with respect to the mole fraction cholesterol indicates this mesogenic system was behaving as a single compound and thus follows the rule of additivity proposed by Diele [17].

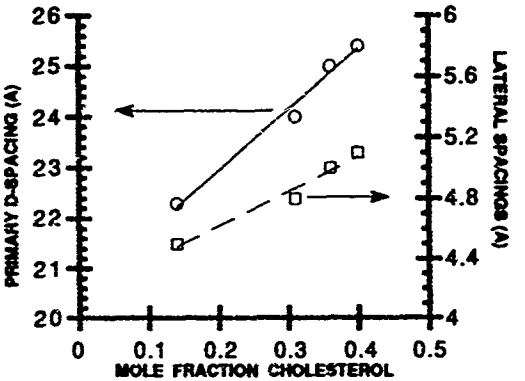

Figure 26: Linear dependence of primary d-spacings and lateral spacings with mole fraction cholesterol

He has shown that some mixtures containing mesogens of different lengths show only one Bragg reflection which is governed by Equation 3:

$$d = x_1 * L_1 + x_2 * L_2. \qquad \text{Eq. 3}$$

These observed reflections vary linearly with the average of the individual extended molecular lengths of each mesogen, L_1 and L_2. This behavior is expected when a mixed mesogen system behaves statistically as one (i.e., there are no intermolecular phase differences between mesogens). The linear dependence of the primary d-spacings for these materials suggests the packing behavior responsible for the lamellar-like structure was due to a statistical average of the two mesogens present within the ring system.

Based on the size of this primary d-spacing and the higher order layer lines, a model (Figure 27) consisting of highly interdigitated mesogens delineated by the central siloxane rings has been proposed. In this model, the mesogens show a high degree of interdigitation with respect to one another analogous to the mixed mesogen system discussed above. Between the mesogens, the cyclic siloxane ring is positioned in a thin interface (<5 Å) of siloxane-rich material. Due to chemical dissimilarities between this siloxane-rich interface and the hydrocarbon regions, a "microphase" separation induces a lamellar-like structure. These striations give rise to long-range order atypical of cholesteric materials which presents itself as higher order reflections in the corresponding X-ray patterns. The exact conformation of the cyclic ring in the interface with respect to the mesogenic positions is currently being investigated.

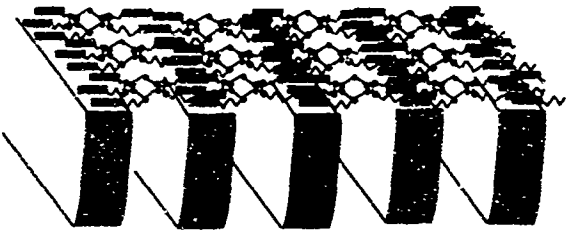

Figure 27: Proposed model of lamellar-like structure

Normal X-ray diffraction behavior

X-ray patterns taken normal to a film surface exhibit uniform azimuthal intensity rings with the same d-spacings as observed with the edge samples. WAXS normal patterns of compounds 1 and 4 are shown in Figures 28 and 29. As discussed earlier, these materials are cholesteric on a macromolecular scale with the helical axis normal to the film surfaces. This behavior is induced by the chiral steroid molecules which cause slight rotation of each subsequent layer as they traverse through a film. As an X-ray beam passes through the film (parallel to helical axis), it sees all possible orientations of the molecules and thus generates even intensity rings similar to a powder pattern.

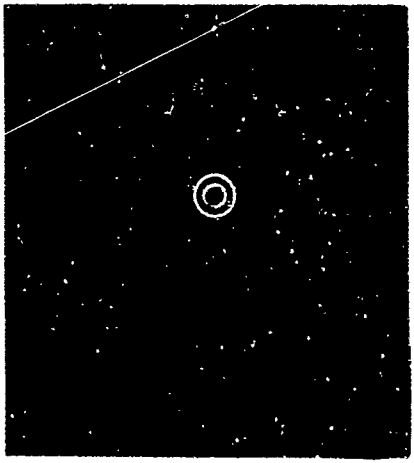

Figure 28: Typical normal WAXS diffraction pattern of compound 1

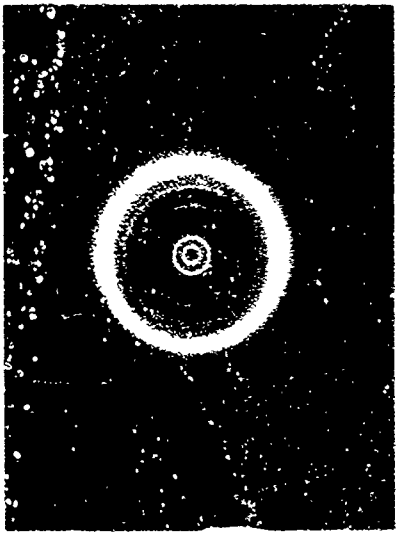

Figure 29: Typical normal WAXS diffraction pattern for compound 4

The model discussed earlier can be extrapolated to a macromolecular scale as shown in Figure 30. The individual lamellae slowly twist on a molecular scale giving rise to the macromolecular twist (normal to the film substrates) typical of cholesteric materials.

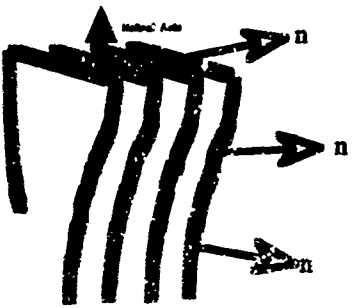

Figure 30: Macroscopic helical twist of lamallae induced by chiral mesogens

SAXS Results

Also shown in Table 5 were low-angle reflections (50 Å) observed on the meridian for both edge and normal geometries. Small-angle data were obtained using a sample-to-film distance of 170 mm. A typical small-angle pattern, shown in Figure 31, shows the primary layer reflection, the third order layer line, and a diffuse low angle reflection. The intensity of the 2nd order layer line was too small in some instances to be observed. The intensity on the equator near the beam stop is typically attributed to "void" scattering, where a horizontal streak corresponds to axially (vertically) elongated voids.

Figure 31· Typical small-angle diffraction pattern (compound 4)

Unlike the primary layer spacings, there was no dependence of this low-angle spacing with x_{chol}. There was, however, a strong intensity dependence of this reflection with mole fraction cholesterol. As Figure 32 shows, the small angle reflection became weaker compared to the normalized primary layer reflection as x_{chol} was decreased. Compound 1 exhibits a strong low angle reflection while compound 4 exhibits no low angle reflection. This trend, coupled with the nondependence of this spacing on x_{chol}, indicates this reflection was caused by regions where the cholesterol mesogens could not become fully interdigitated as previously shown in Figure 27. Figure 32 suggests the frequency of the packing domains causing this low-angle reflection increased with an increase in x_{chol}. This

increased frequency disrupts the long-range order of the highly interdigitated regions as shown in Figure 33. Compound 4 clearly exhibits four layer lines with a marked absence of the small-angle reflection. Contrary to this behavior, compound 1 clearly shows the presence of a strong small-angle reflection and very weak higher order layer lines. This behavior indicates a shift in the packing behavior which was strongly dependent on the mole fraction cholesterol. The presence of strong 2nd and 4th order layer lines in addition to 5th and 6th order lines indicates compound 4 possesses long-range order to a greater degree than the other three materials.

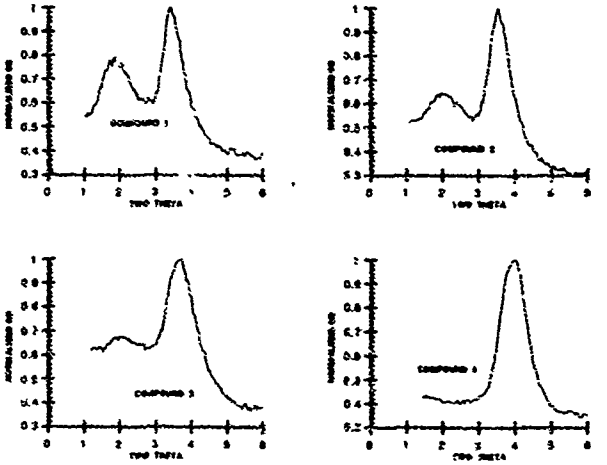

Figure 32: Intensity variations of small-angle reflections with respect to mole fraction cholesterol

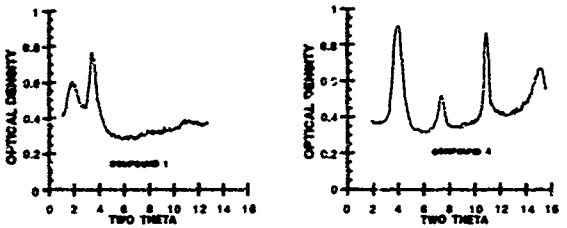

Figure 33: Disruption of long-range order based on SAXS

The domination of cholesterol in the packing structure of liquid crystalline polymers has been observed before by Freidzon [18]. With cholesterol containing acrylate and methacrylate polymers (>30%), he observed packing structures with various degrees of interdigitation depending on the length of the leader group. Specifically, when medium length leader groups were used to attach cholesterol to the backbone, both a highly ordered interdigitated packing structure and a less ordered structure were observed. The highly interdigitated structure corresponded closely to the molecular length of the mesogen plus the backbone. The less ordered packing structure was attributed to the partial overlap of the cholesterol mesogens. Due to steric hinderances, the cholesterol mesogens were only allowed to superimpose their aliphatic tails. The measured low-angle reflection corresponded closely to the calculated extended end-to-end molecular dimensions of this model. Decreasing the length of the leader group resulted in a greater frequency of this low-angle reflection as the decreased flexibility increases the steric interactions. Conversely, increasing the length of the leader group

decreased the frequency of this less ordered structure and the highly interdigitated structure became dominant.

In comparison, the packing behavior observed with the Wacker LC-Silicones is analogous, as two types of packing, one a highly interdigitated structure and the other a less ordered structure, were present. With the low x_{chol} material (x_c=0.14), the system behaves as a single component where the mesogens are forced apart into a highly layered structure due to the cyclic siloxane ring. As more and more cholesterol is added to the material, it disrupts the highly interdigitated structure as it is sterically unable to "squeeze" into the layered structure. Instead, it forms regions where cholesterol cannot interdigitate and thus a larger (low-angle) spacing was observed. As the frequency of these regions increases, they disrupt the continuity of the long-range order which was evidenced by the weaker higher order layer lines in the higher x_{chol} samples.

Fiber Diffraction

As mentioned previously, the fiber drawing capabilities of these materials is unique due to their low molecular weights. Glassy fibers of various diameters were investigated with WAXS and SAXS geometries shown in Figure 34. X-ray patterns taken from fibers resemble those of the film edge as shown in Figure 35. The higher order layer lines residing on the meridian suggest the mesogens were aligned parallel to the fiber direction and subsequently the lamellar structure was perpendicular to the fiber axis. This behavior was partially confirmed with SEM as discussed earlier. This is contrary to most fiber patterns of side-chain liquid crystalline polymers where the backbone is typically aligned parallel to the

fiber direction with the side-chain mesogens aligned perpendicular to the fiber axis. Although this material is a side-chain liquid crystalline material, on a macroscopic scale, it resembles a main-chain liquid crystalline material where the interdigitated chains are parallel to the fiber direction. It is hypothesized that as the material was drawn, the cholesteric helix was untwisted to give a fiber with uniaxial order. The high degree of interdigitation among mesogens along the fiber direction perhaps imparts enough longitudinal (tensile) strength to the materials to allow fibers to be drawn.

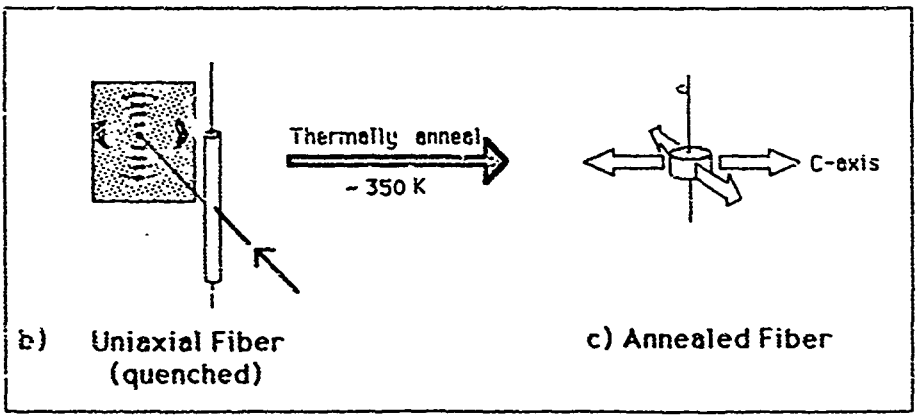

Figure 34: X-ray diffraction geometries used with fibers

Figure 35: Typical WAXS pattern of fiber-compound 4

Elevated Temperature X-ray Results

Powder diffraction patterns for two of the Wacker LC-Silicones were obtained at a series of temperatures to confirm that the X-ray reflections observed from the glassy film and fiber samples were not a manifestation of the glass. Compound 1 was examined at successive temperatures of 25°C, 100°C, 160°C, and 230°C while compound 4 was examined at 25°C, 155°C, 165°C, 200°C, and 230°C, and 100°C. These temperatures span from the glassy state to above the clearing temperatures. Figures 36-39 show the behavior of compound 4 as it was heated from the glassy state (25°C), to the

liquid crystalline phase (165°C), to the isotropic state (230°C), and finally cooled back to the liquid crystalline phase (109°C). Upon heating into the isotropic phase, the wide-angle halo attributed to the liquid-like motions of the mesogens become very diffuse while the other reflections disappear. Upon cooling below the clearing point, the reappearance of these X-ray reflections suggest they are indeed due to inherent structure present within the liquid crystalline mesophase.

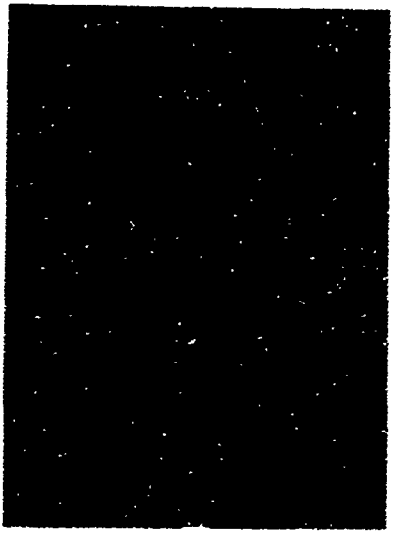

Figure 36: Compound 4 at 25°C

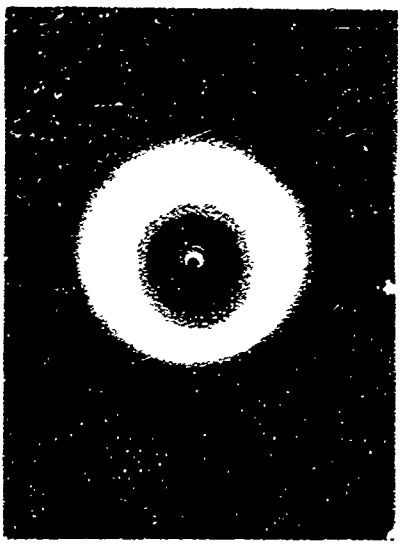

Figure 37: Compound 4 at 165°C

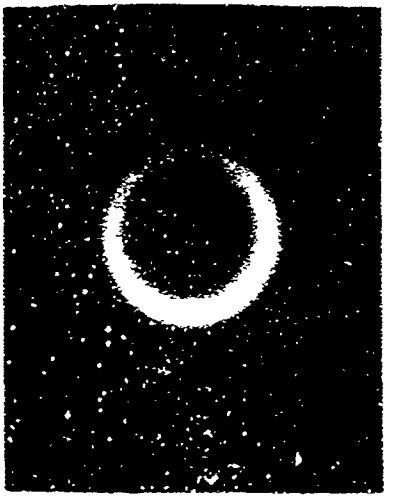

Figure 38: Compound 4 at 230°C

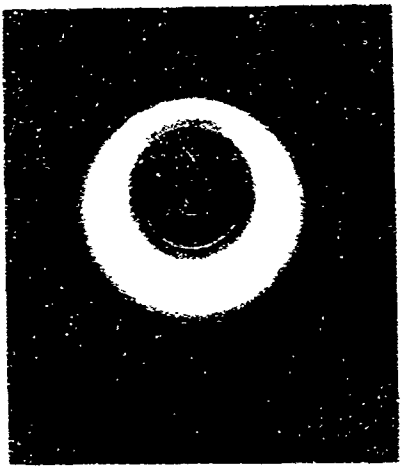

Figure 39: Compound 4 at 100°C

The X-ray patterns for both compounds taken from within the liquid crystalline region compare very well to those taken at room temperature. A slight lengthening (≈1.0Å) of the primary d-spacings (as well as the lateral spacings) with temperature was observed for both compounds as shown in Tables 6 and 7. The lateral spacings also increased slightly with temperature. This was attributed to the increased mobility (liquid-like motion of mesogens) as the temperature was increased. The behavior of the low angle reflection could not be observed because of the short sample-to-film distance.

Table 6

Spacings as a Function of Temperature for Compound 1

T (°C)	d-spacing (Å)	Lateral spacing (Å)
25°C	24.9	5.2
100°C	25.9	5.25
160°C	26.1	5.4
230°C	---	very diffuse

Table 7

Spacings as a Function of Temperature for Compound 4

T (°C)	d-spacing (Å)	Lateral spacing (Å)
25°C	21.6	4.5
155°C	21.9	4.7
165°C	22.2	5.1
200°C	---	5.1
230°C	---	5.1
100°C	22.2	4.6

Microcamera results

Several attempts were made to examine individual thin fibers (<30μm) using a microcamera. Fibers of compounds 1 and 4 were examined. These fibers were accidently formed when spin coating the Wacker LC-Silicones onto glass substrates using an in-house spin coater. Fibers were observed to form as individual filaments exited the glass substrates radially and subsequently became wrapped around the rotor. The very fast rotation formed mats of thin fibers with a consistency similar to cotton candy as shown in Figure 40. Groups of these fibers were first examined by pulling them roughly uniaxial and examining these with a Statton camera (50 mm). These mats show X-ray patterns (Figures 41 and 42) similar to individual hand-drawn fibers. Again, there were multiple order reflections on the meridian suggesting liquid crystalline order parallel to the fiber axes.

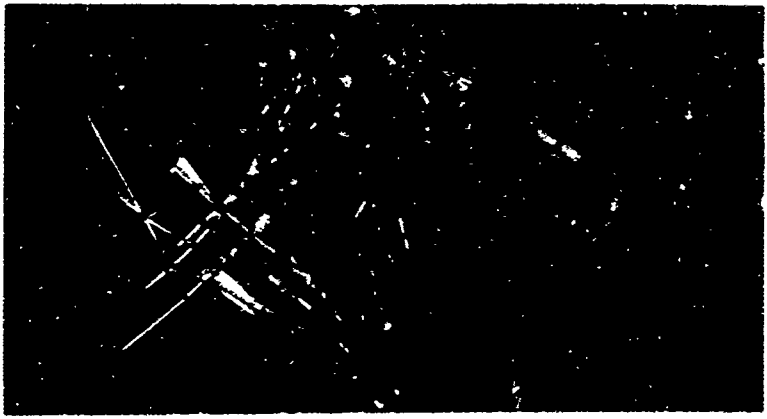

Figure 40: Thin fibers as observed under crossed polarizers

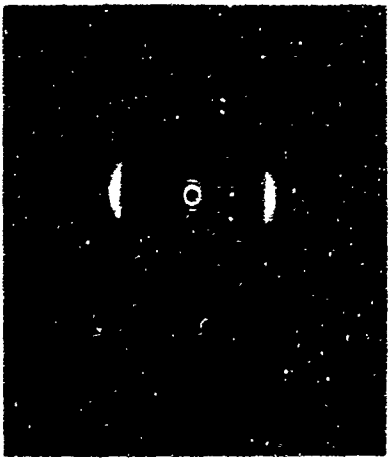

Figure 41: Diffraction pattern from group of fibrils of compound 1

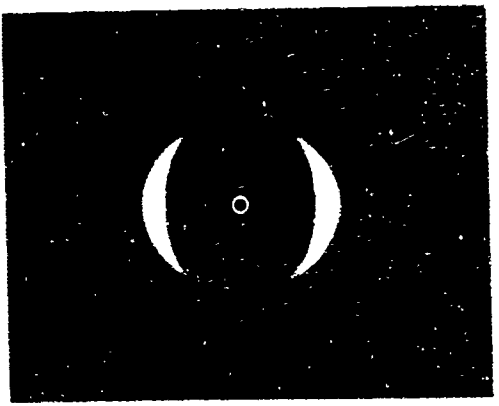

Figure 42: Diffraction pattern from group of fibrils of compound 4

Individual filaments (<30μm) from these spun coat fibers were examined with a microcamera to investigate the relative ordering with respect to the mats of fibers shown in Figures 41 and 42. Specifically, do the individual filaments possess exceptional ordering because of the high shear it was subjected to in the fiber formation process? Individual fibers were mounted in the microcamera and exposed for 24-72 hours on the KU-2600 generator. The resulting patterns obtained for compounds 1 and 4, Figures 43 and 44, show less ordering than the mats of fibers. The orientation of the individual filaments is shown by the arrow. These figures clearly show poor orientation as almost concentric rings were observed. There was some orientation exhibited as demonstrated by the larger equatorial crescents but much less than that exhibited in Figures 41 and 42. This behavior was unexpected as thin filaments from a group of fibrils typically exhibit better alignment than the group itself.

Possible explanations include some sort of X-ray beam heating which because of the very thin diameters shrinks and relaxes the fibers. This elastic behavior has been observed with hand-drawn fibers which when heated to 60°C, quickly shrink into a random blob thereby losing their uniaxial order. As discussed previously, TEM/SEM results have indicated that the orientations of fibrils in these shrunken materials was fairly random, similar to a focal-conic texture.

Another possible explanation was the relaxation of the uniaxial order with time. Roughly 6 months had passed from the time when the fibers were accidently drawn and initially examined (Figure 41

and 42) with the Statton camera and then finally examined with the microcamera. Due to the low T_g's of these materials, perhaps over time the molecules have enough mobility to slowly relax. To date, no more work has been performed on these "cotton" candy samples. Still, the ability of these materials to be drawn into very thin, highly birefringent fibers leads to possible NLO fiber applications.

Figure 43: X-ray pattern from an individual filament of compound 1

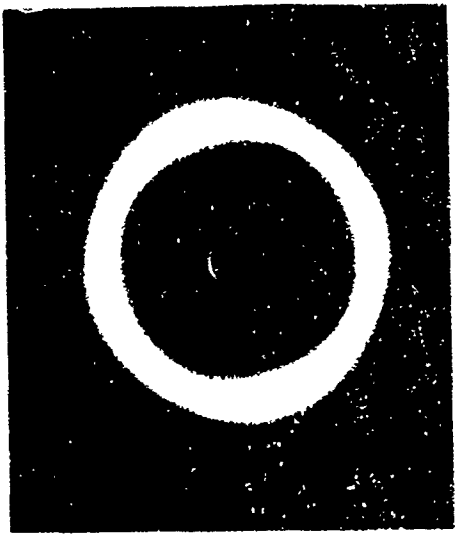

Figure 44: X-ray pattern from an individual filament of compound 4

Fixed-end Fiber Results

It has been shown by others that annealing fibers of a semi-crystalline nature at elevated temperatures near the T_g can cause an increase in crystallinity. This has been especially true for polyethylene materials. This increase in order is due to an increase in the relative proportions of crystalline/amorphous regions within the fiber. By fixing the fiber ends, the long polymer chains align parallel to the fiber direction when enough energy is imparted to induce thermodynamic mobility.

This same type of behavior was examined for a thin fiber of compound 1. A WAXS pattern was taken with the Statton camera and this same fiber was then annealed at 56°C, slightly above its T_g for 12 hours. Figures 45 and 46 show the before and after WAXS

patterns taken from this fiber. The ordering seems to have decreased as evidenced by the broader arcs in the latter figure. This was not unexpected as thermodynamically these materials do not resemble the typical fiber materials usually applied to this type of treatment. For these materials, being pulled into a fiber is not by far their most favorable thermodynamic state. This has been shown previously in this report as heating fibers above their T_g causes an immediate relaxation into the focal-conic texture. It was thus not surprising that the order decreased upon annealing as the material fights to leave the uniaxial packing structure induced on drawing.

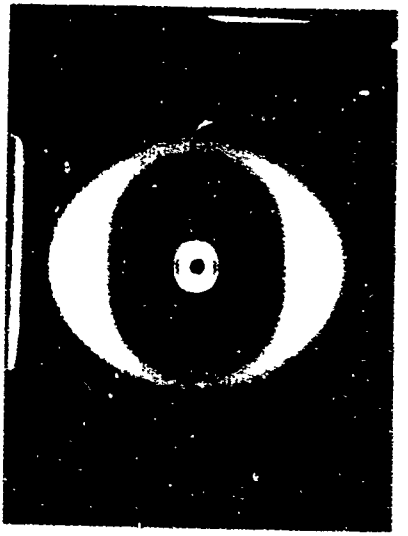

Figure 45: Fiber pattern of compound 1 before annealing

Figure 46: Fiber pattern of compound 1 after annealing

CONCLUSIONS

Side-chain liquid crystalline materials offer the possibility of enhanced nonlinear optical properties due to their processability and their inherent ability to order. A cyclic siloxane-based cholesteric liquid crystalline system was initially examined using electron and optical microscopy, X-ray diffraction, and spectroscopy. These materials consist of a 5-membered cyclic siloxane core with cholesteryl-4-allyloxybenzoate and biphenyl-4-allyloxybenzoate mesogens attached. The ratio of the two mesogens can be controlled to selectively reflect light from the UV to the NIR.

These materials exhibit several unusual properties including the ability to be drawn into fibers. These fibers exhibit uniaxial order with the lamellae oriented perpendicular to those within most conventional polymeric liquid crystalline fibers. Electron microscopy indicates an absence of a mature cholesteric twist within the fibers.

X-ray diffraction examinations reveal molecular order atypical of conventional liquid crystalline materials. Thin film edges and fibers exhibit 4-6 layer reflections indicating unusually well defined long-range uniaxial order. The d-spacing of the primary layer reflections indicates a highly interdigitated mixed mesogen system with a thin interface of siloxane separating hydrocarbon regions. The addition of more cholesterol mesogen seems to disrupt the long range order.

REFERENCES

1.) Williams, D.J., (ed.), Nonlinear Optical Properties of Organic and Polymeric Materials, ACS Symp. Ser. 233, American Chemical Society, Washington, D.C., 1985.

2.) Chemla, D.S., and Zyss, J., (eds.), Nonlinear Optical Properties of Organic Molecules and Crystals, Academic Press, Orlando, Vols. I and II, 1987.

3.) Mohlmann, G.R., and van der Vost, C.P.J.M., in Side Chain Liquid Crystal Polymers, C.B. McArdle (ed), Blackie and Son, Glasgow/Chapman and Hall, N.Y., 1989.

4.) Krishnamurthy, S. and Chen, S.H., Makromol. Chem., **190**, 1407(1989).

5.) Tsai, M.L., Chen, S.H., and Jacobs, S.D., Appl. Phys. Lett., **54(24)**, 2395(1989).

6.) Pinsl, J., Brauchle, Chr., and Kreuzer, F.H., J. Mol. Elect., **3**, 9(1987).

7.) Ortler, R., Brauchle, Chr., Miller, A., and Riepl, G., Makromol. Chem., Rapid Commun., **10**, 139(1989).

8.) Bunning, T.J., Klei, H.E., Samulski, E.T., Linville, R.J., and Crane, R.L., Liq. Cryst., (1991), In press.

9.) Provide by F.H. Kreuzer of the Consortium fur Electrochemische Industrie of West Germany.

10). Data sheet provided with Wacker LC-Silicones.

11). DeVries, H.L., Acta. Cryst., **4**, 219(1951).

12.) Takezoe, H., Hashimoto, K., Ouchi, Y., Hara, M., Fukuda, A., and Kuze, E., Mol. Cryst. Liq. Cryst., **101**, 329(1983).

13.) Hara, H., Satoh, T., Toya, T., Iida, S., Orii, S., and Watanabe, J., Macromolecules, **21**, 14(1988).

14). Ballauf, M., aand Schmidt, G.F., Makromol. Chem., Rapid Commun., **8**, 93(1987).

15.) Mugge, J., and Zugenmaier, P., Mol. Cryst. Liq. Cryst., **155**, 409(1988).

16.) Leadbetter, A.J. in Thermotropic Liquid Crystals, Gray, G.W. (ed.), Critical Reports on Applied Chemistry, Vol. 22, Ch. 1, John Wiley, 1987.

17.) Diele, S., and Sackmann, H., Ber. Bunsenges. Phys. Chem., **93**, 467(1989).

18.) Freidzon, Ya. S., Kharitonov, A.V., Shibaev, V.P., and Plate, N.A., Eur. Polym. J., **21**(3), 211(1985).